Journal of Energy Chemistry 26 (2017) 466–475

Contents lists available at ScienceDirect

Journal of Energy Chemistry

journal homepage: www.elsevier.com/locate/jechem

http://www.journals.elsevier.com/journal-of-energy-chemistry/

Hydrogen evolution kinetics on Ni cathodes modified by spontaneous deposition of Ag or Cu

Esteban A. Franceschini[a,*], Gabriela I. Lacconi[a], Horacio R. Corti[b,c]

[a] INFIQC-CONICET, Departamento de Fisicoquímica – Facultad de Ciencias Químicas, Universidad Nacional de Córdoba, Ciudad Universitaria, 5000 Córdoba, Argentina

[b] Departamento de Física de la Materia Condensada, Centro Atómico Constituyentes, Comisión Nacional de Energía Atómica, Av. Gral. Paz 1499 (B1650KNA) San Martín, Buenos Aires, Argentina

[c] INQUIMAE-CONICET, Facultad de Ciencias Exactas y Naturales, Universidad de Buenos Aires, Ciudad Universitaria, Pabellón II, C1428EHA, Buenos Aires, Argentina

ARTICLE INFO

Article history:
Received 12 September 2016
Revised 21 October 2016
Accepted 27 October 2016
Available online 18 November 2016

Keywords:
Hydrogen evolution reaction
Spontaneous deposition
Nickel/Silver
Nickel/Copper
Electrochemical impedance spectroscopy

ABSTRACT

Nickel modification by spontaneous deposition of transition metals such as Ag and Cu is shown as an economic and simple alternative for the activation of hydrogen evolution reaction (HER) on cathodes in alkaline media. The kinetics of HER is studied on Ni/Ag and Ni/Cu catalysts by cyclic voltammetry and electrochemical impedance spectroscopy (EIS) using a rotating disk electrode (RDE). Freshly synthesized catalysts, as well as catalysts subjected to a short chronoamperometric ageing procedure, are analyzed and the kinetic and thermodynamic parameters of the HER are obtained. The nickel surface modified with transition metals with an outer shell electronic configuration [$xd^{10}(x+1)s^1$], such as Cu ($3d^{10}4s^1$) and Ag ($4d^{10}5s^1$), shows an improved activity for the HER compared to bare nickel. Furthermore, the Ni/Cu catalyst presents a decreased onset potential. The hydrogen evolution rate, measured as current density at −1.5 V (vs. SCE), is similar on Ni/Cu and Ni/Ag electrodes.

1. Introduction

Hydrogen is considered one of the most promising alternatives as an energy vector for the future [1–4]. Hydrogen production methods that do not generate greenhouse gases emission are of great interest, being the water electrolysis in alkaline medium one of the most interesting. Since the hydrogen evolution reaction (HER) is an heterogeneous reaction, the electronic state of the electrode surface plays a dominant role in determining the reaction kinetics. In the last decades, numerous research articles have been published on the mechanism of the HER on promising electrocatalysts, such as nickel alloys [5–10] and complex materials [11–15], and one of the most important conclusions is that the reaction rate of the HER should depend on the hydrogen binding energy on the given metal [16].

It is well known that a good catalyst requires an adsorption free energy, ΔG_{ad}, as small as possible, a D-band that permits to span the Fermi level, and a strong long-range interaction between the catalystś bands and the hydrogen 1*s* orbital. It's important to note that a too weak binding to the surface will result in poor adsorption of the reactant retarding the reaction, whereas a too strong binding will originate a difficult removals of the final products. In this way, the metals used for the modification of the electrode should present a proper adsorption free energy in order to reach a synergistic effect favoring the hydrogen evolution reaction. Additionally, a long-range interaction is important because the electron transfer to the proton occurs at a distance in the order of 0.5 Å from the adsorption site [17]. Copper, with $\Delta G_{ad} = 0.1$ eV, should be an excellent catalyst. However, as a third row element, the orbitals of copper are compact; therefore the overlap with the hydrogen 1*s* orbital is short-ranged. In the case of Ag, the position of the D-band is less favorable therefore the coupling between the catalyst bands and the H 1*s*-band is weaker [18], and the energy of adsorption is less favorable for Ag ($\Delta G_{ad} = 0.39$ eV) compared to Cu.

A few previous works on Ni modified with Cu or Ag are reported in the literature exploring different synthesis methods. In a pioneer work, Conway et al. [19] studied the electrochemical kinetics of hydrogen evolution in different commercial copper–nickel alloys. He found that the apparent activation energy of the alloys decreased with increasing concentration of copper, while the current densities showed an opposite trend.

* Corresponding author. Fax: +54 11 6771 7121.
E-mail addresses: efrances@tandar.cnea.gov.ar, estebanfranceschini@yahoo.com.ar (E.A. Franceschini).

http://dx.doi.org/10.1016/j.jechem.2016.10.009

Sharifi-Asl and Macdonald [20] have investigated the effects of temperature, pH, and hydrogen pressure on the kinetics of the HER on Cu electrodes in order to obtain the kinetic parameters (exchange current density, Tafel slope and activation energy). The mechanism of the HER, studied by electrochemical impedance spectroscopy (EIS), indicated that the Volmer reaction is the rate determining step for the HER on copper in alkaline media.

Yin and Chen [21] synthesized Ni/Cu composites with hierarchical structure by a three steps electrochemical method: galvanic replacement reaction, activation process, and cyclic voltammetry treatment. The galvanic replacement reaction to prepare Ni/Cu precursors consisted in the immersion of Ni foam into copper ion solutions. The results indicate that the optimal dipping time in $CuCl_2$ solution was 1 h. The effectiveness of the nickel modification may be attributed to the adsorption of chloride ion on the copper surface, with the formation and hydrolysis of $CuCl_n^{1-n}$ complex, which promotes the exchange reaction between Ni and Cu^{2+}.

Jaramillo and coworkers [22] synthesized binary Ni/Ag bulk alloys with different compositions and showed that those alloys are indeed more active than pure Ni for the HER. They found that for $Ni_{0.75}Ag_{0.25}$ the hydrogen evolution current per geometric area was approximately double that obtained for pure nickel, and both catalysts exhibited comparable stability. The experimental results were supported by density functional theory calculations, which show that bulk alloying Ni and Ag creates a variety of adsorption sites, some of which have near-optimal ($\Delta G_{ad} = 0$) hydrogen binding energy.

In a previous work we determined the kinetic and thermodynamic parameters of the HER on nickel. It was concluded that in alkaline solution the Volmer reaction is not controlled by water molecules diffusion, but by the diffusion of HO^- ions. Thus, a theoretical Koutechy–Levich (K-L) slope was calculated [23]. In this work, $xd^{10}(x+1)s^1$ metals (Ag and Cu) are deposited on nickel catalysts through a simple and reproducible spontaneous process, with adequated morpohologic and electrochemical characterization. These modified nickel electrodes are analyzed by rotating disk electrode using linear sweep voltammetry at different rotation rates and temperatures, cyclic voltammetry, EIS, and chronoamperometry. Thus, Tafel and catalytic activity toward the HER are performed. The results are compared with those previously obtained for pure nickel [23].

2. Experimental

2.1. Chemicals

Hydrochloric acid 36.5%–37% (Cicarelli, PA grade), potassium hydroxide (Anedra RA reagent), ethanol 96% (Cicarelli, PA grade), copper nitrate (99.99%, Aldrich), and silver nitrate (99.99%, Aldrich) were used as received. All aqueous solutions were prepared with Milli-Q water, and degassed using high purity N_2 (Indura S.A.).

2.2. Catalyst synthesis

The electrodes used for catalysts synthesis were Ni disks (99.9 purity, RC S.A.) with an area of 0.196 cm^2. The electrodes were mechanically polished with 0.05 μm alumina, repeatedly cleaned with ethanol, and then immersed in 1 M KOH aqueous solution, and HCl (10% w/w) aqueous solution, during 1 min, in order to degrease the surface.

The surface modifications were carried out by immersing the freshly polished and degreased nickel electrodes in degassed $AgNO_3$ (1 g dm^{-3}) or $Cu(NO_3)_2$ (1 g dm^{-3}) aqueous solution during 30 min at room temperature. The spontaneous deposition time was selected taking in consideration a previous work in other catalysts synthesized in a similar way [24]. The Ag or Cu deposition occurs through a displacement reaction where Ni is dissolved while the second metal is deposited.

The cell voltage measurement during the synthesis of the electrodes was performed in a two electrode cell using a platinum foil as counter electrode. Ni/Ag catalyst was synthesized without a reference electrode, to avoid changes of silver ions concentration by the presence of chlorides and subsequent AgCl formation. Ni/Cu catalyst was synthesized in the same conditions with comparative purposes. Silver and copper deposition occurs in the same way when the synthesis is carried out without Pt counter electrode and cell voltage measurement.

2.3. Structural characterization

Scanning electron images were obtained using a Supra 40 (Zeiss Company) FESEM operating at 3 kV, equipped with EDX. EDX spectra and EDX mapping were obtained operating at 6 kV.

X-ray diffractograms were measured employing the Cu $K\alpha$ radiation ($\lambda = 1.5406$ Å), using a PANalytical X'Pert PRO diffractometer (40 kV, 40 mA), in the θ–2θ Bragg–Brentano geometry at room temperature. A 2θ range between 10° and 70° was selected, with increments of 0.02° and a counting time of 14 s per step. The FULLPROF program [25] was applied to refine the crystal structure by the Rietveld method. A pseudo-Voigt shape function was used to fit the experimental data. The data refined were atomic positions, lattice parameters, peak shape, isotropic thermal parameters, and occupation factors.

2.4. Electrochemical characterization

Electrochemical characterization of the electrodes was conducted in a conventional three-electrode cell with a thermostatic jacket, and the temperature was varied between 278 K and 303 K in 5 K steps, controlled using a Lauda Alpha RA 8 thermostat. A large area platinum foil was used as counter electrode, and a saturated calomel electrode (SCE) as reference electrode (0.243 V vs. RHE). The reference electrode, immersed in a capillary with gel, was kept outside the cell at room temperature. 1 M KOH aqueous solution was used as electrolyte. In order to avoid diffusion of KCl from the reference electrode through the agar membrane, we have used an external glass sheath with a platinum wire at the end. Electrochemical studies were carried out employing an Autolab PGStat30 potentiostat/galvanostat with FRA2 module, coupled to a rotating disk electrode system (Pine Research Inst.; Raleigh, NC). The uncompensated ohmic drop (~50 Ω) was measured via high frequency ac impedance in N_2 saturated 1 M KOH, and used to measure the cell ohmic drop. The ohmic drop correction to the applied potentials was made automatically by Autolab software (Metrohm Autolab Nova 1.10). Rotating disk electrode (RDE) measurements were conducted on Ag and Cu modified Ni disk electrodes mounted in an interchangeable RDE holder (Pine Research Inst.; Raleigh, NC) and the rotation rate was varied between 100 and 2500 rpm.

Cyclic voltammetry (CV) and linear sweep voltammetry (LSV) experiments were conducted between 0.1 and −1.5 V (vs. SCE) for all catalysts at a scan rate of 10 mV s^{-1}.

EIS experiments were conducted by applying a bias of 10 mV at frequencies between 10 mHz and 50 kHz at different electrode potentials such as, open circuit potential (OCP), HER onset potential (OP), and 0.1 V and 0.3 V overpotentials more cathodic than the corresponding OP of each catalyst. Chronoamperometric measurements were carried out applying −1.5 V (vs. SCE) during 4 h at 298 K. EIS and chronoamperometric experiments were carried out by rotating the electrode at 900 rpm to prevent the formation of bubbles. Additionally, after each CV the electrode was rotated at

1600 rpm to prevent the formation and accumulation of bubbles occluding the surface of the electrodes.

During all electrochemical measurements a nitrogen flux was maintained above the electrolyte surface.

2.5. Electrochemical analysis

There are different parameters for testing the catalytic activity of an electrode in relation to a particular reaction. The simplest is the current density, but it is strongly influenced by parameters such as the exchange current (j_0) and the dj/dV slope. The OP is presented as an important factor since for the same dj/dV gradient, the catalyst with a lower OP presented higher current density and therefore, greater catalytic activity.

The electrochemical analysis was carried out as reported elsewhere [23,26]. The HER overall current density (denoted as j) can be represented by the Koutecky–Levich (K–L) equation [26]:

$$\frac{1}{j} = \frac{1}{j_k} + \frac{1}{j_d} = \frac{1}{j_k} + \frac{1}{B\omega^{1/2}} \quad (1)$$

where j_k is the kinetic current density, j_d the boundary-layer diffusion limited current density, ω is the rotation rate (rpm) and B is the Levich slope ($mA^{-1}\,cm^2\,rpm^{1/2}$) given by,

$$B = 0.2nFC_oD_o^{2/3}n^{-1/6} \quad (2)$$

where 0.2 is a constant used when ω is expressed in rpm, n is the number of electrons transferred per molecule of H_2O reduced, F the Faraday constant (96,485 C mol^{-1}), C_O is the HO^- concentration in the solution (0.001 mol cm^{-3}), D_O is the HO^- diffusion coefficient (5.3×10^{-5} $cm^2\,s^{-1}$) [27], and ν the cinematic solution viscosity (9.473×10^{-3} $cm^2\,s^{-1}$) [27]. The theoretical value of B for single electron charge transfer (i.e., $n = 1$) process is 59.20 mA cm^{-2} $rpm^{-1/2}$ [23]. The calculated B slope for all catalysts was compared with the theoretical B value, permitting us to evaluate the number of electrons involved in the reaction.

The kinetic current density (j_k), was calculated by correcting the current density (j) by the mass transfer using the diffusional limiting current (j_d) as showed elsewhere [23,26].

The kinetic current density is used to construct Tafel plots, and by the use of the Tafel equation (Eq. (3)) it was possible to obtain the exchange current (j_0) and the Tafel slope (b).

$$\log j_k = bE + j_0 \quad (3)$$

Additionally, Tafel slope can be defined as:

$$b = \frac{2.3RT}{F\alpha} \quad (4)$$

where α the transfer coefficient. In order to calculate the value of n (number of electrons transferred), an α value of 0.5 is used. It is important to note that this value of $\alpha = 0.5$ is theoretical and is used only as an estimate in order to be able to infer the Tafel slope and thus the RDS. As a consequence, the n presented values are not integers.

3. Results and discussion

3.1. Catalysts synthesis

During the preparation of Ni/Ag and Ni/Cu electrodes, the spontaneous deposition of Ag and Cu is monitored measuring the OCP. Fig. 1 shows the variation of OCP vs. deposition time for the two catalysts. In both cases the OCP is initially negative, which is consistent with a displacement reaction where Ni is oxidized, while the second metal (Ag or Cu) is reduced and deposited on the electrode surface. It can be seen that the OCP for Ni/Ag and Ni/Cu catalysts differs by ~0.4 V, and the difference increases with time,

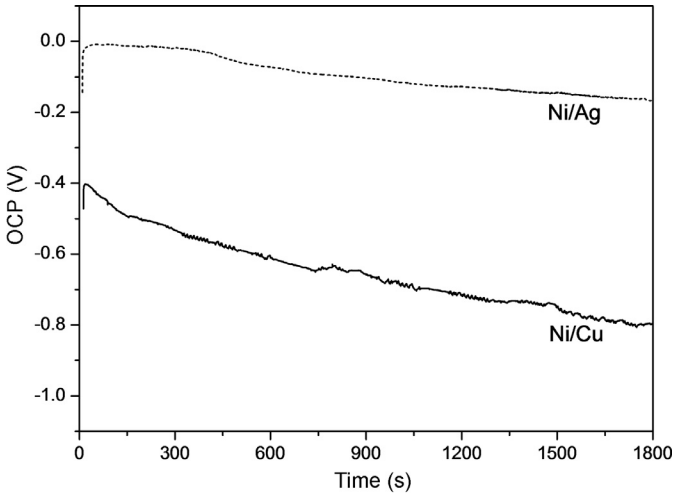

Fig. 1. OCP as a function of time for fresh cleaned Ni samples immersed in 1 g dm^{-3} $AgNO_3$ solution (filled curve) and 1 g dm^{-3} $Cu(NO_3)_2$ solution (dashed curve).

reaching 0.63 V after 1800 s (at the end of synthesis), as a result of the chemical changes produced on the electrodes surface. Both OCP decrease during the catalyst synthesis and while Ni/Ag catalyst reach a steady state with an OCP change of 0.16 V, Ni/Cu catalyst shows a major change in the OCP (ca. 0.4 V) in the same time range.

3.2. Structural characterization

Scanning electron micrographs were obtained in order to analyze the electrode structure, and the presence of crevices. Fig. 2(a) shows the SEM micrograph of a freshly synthesized Ni/Ag sample (Ni/Ag_f) at 100.000 × magnification (higher magnification SEM micrographs are presented in Fig. S1a and b in Supplementary Material). The sample is mainly granular and shows polishing marks. No surface fractures are observed. In Fig. 2(b) and (c) SEM images of a freshly synthesized Ni/Cu sample are shown. In this case, the presence of cubic shaped particles is mostly observed.

Moreover, back-scattered electron images were taken in order to study the surface area covered by the Ag and Cu particles on the Ni surface (not shown). The image J program was used to obtain the degree of coverage. The Ni/Cu electrode has 18.6 ± 2.1% of the area covered with Cu particles, while in the case of Ni/Ag, 14.2 ± 0.6% of the electrode is covered by homogeneously distributed Ag particles, in 1800 s. The measured average particle sizes are around 250 nm and 400 nm for Ni/Ag and Ni/Cu electrodes, respectively. Considering the mean size of the particles, the degree of coverage aforementioned and the bulk density of Ag and Cu we could estimate average surface loadings of ~4 μg cm^{-2} for Ag, and ~6 μg cm^{-2} for Cu. Due to the difficult of measuring the electrochemical area of nickel electrodes, all current values were normalized to the geometric area of the Ni electrode [28,29].

Nowadays, there is extensive literature describing how copper oxides grow with cubic or octahedrical shape, depending on the synthesis conditions. The differences in the particles shape are due to the different stabilities of the copper oxides (1 0 0) or (1 1 1) crystal planes. Under conditions where the copper oxides (1 0 0) plane is more stable than the (1 1 1), cubic structures, as those seen in Fig. 2(b) and (c), are formed [30,31].

EDX spectra (Fig. S2a and b in the Supplementary Material) have the typical Ni Lα band (0.851 keV) without metallic contamination and only traces of Al and Si (from the alumina polishing) are present. The Ag Lα band at 2.984 keV can also be seen although it is much less intense than the Ni bands. This is because

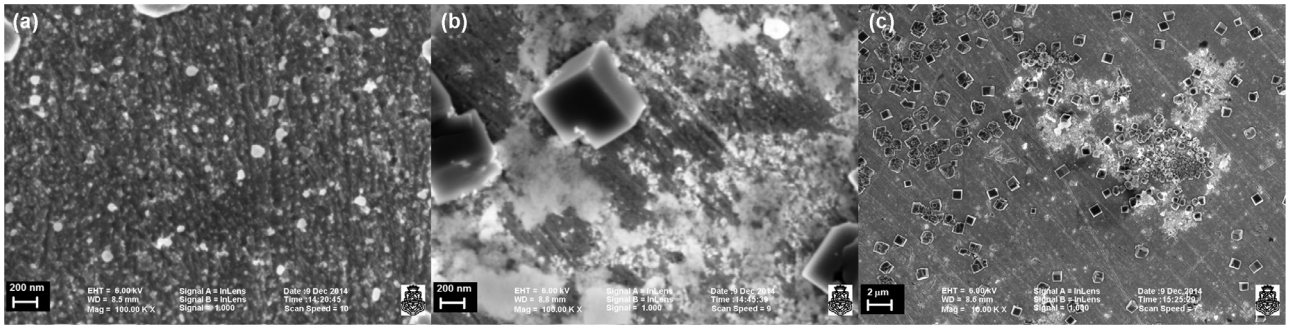

Fig. 2. (a) SEM micrograph of Ni/Ag_f (Magnification of 100,000×) and SEM micrographs of: (b) Ni/Cu_f measured at 6 keV and a magnification of 100,000× and (c) Ni/Cu_f measured at 6 keV and a magnification of 10,000×.

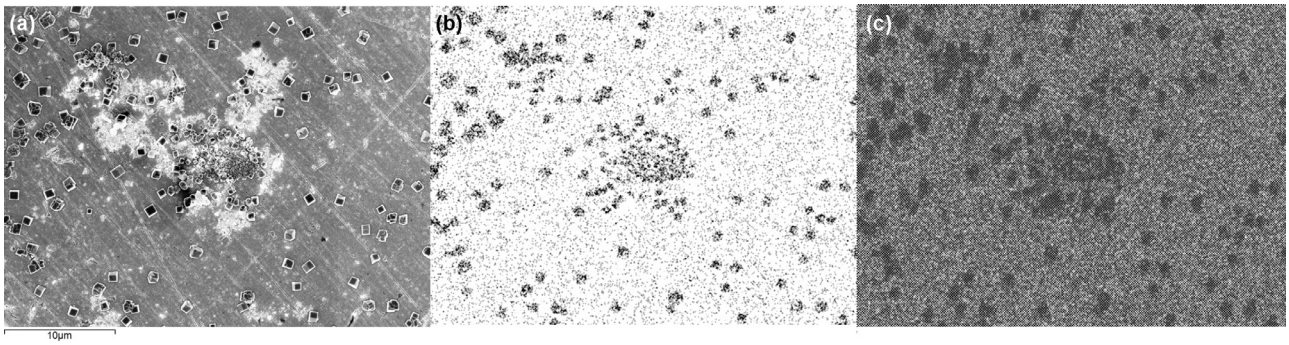

Fig. 3. (a) SEM image on the Ni/Cu catalyst of the zone where the EDX mapping is carried out, (b) EDX mapping of Cu Lα signal and (c) EDX mapping of Ni Lα signal. Magnification of 10,000×.

the EDX beam has high penetration in the material and Ag particles are deposited only on the surface. In the Ni/Ag sample, the EDX mapping (not shown) presents a homogeneous composition in all the sample's surface.

The Cu $K\alpha$ band (8.040 keV) is close to the Ni $K\alpha$ band (7.471 keV) making it difficult to the correct quantification while the Cu Lα band (0.930 keV) has very low intensity and is not quantifiable. So that, the correct quantification of the Cu amount on the sample cannot be carried out by EDX.

Fig. 3(a) shows a SEM micrograph of the Ni/Cu electrode on which the EDX mapping was carried out. Fig. 3(b) presents the Cu signal on the EDX map and shows that the cubes present on the surface are formed by Cu and also the presence of O on the cubes is observed (not shown). In Fig. 3(c) the spatial distribution of Ni on the electrode surface is shown. It is observed that in the areas where Cu particles are present, the intensity of the Ni signal is less intense than the signal in areas without the particles, indicating that, although the Ni Kα and Cu Kα peaks are close together, the elements can be distinguished. EDX mapping of the Ni/Ag (not showed) presents a similar behavior to the observed in the Ni/Cu catalyst.

The X-ray diffraction patterns (Fig. 4) for Ni/Ag_f and Ni/Cu_f clearly show the typical reflections expected for nickel with face centered cubic (fcc) structure. Both samples show peaks at 38.5° and 65.0° corresponding to the Al sample holder.

The values of 2θ for the Ni (1 1 1) and (2 0 0) planes are 44.6° (FWHM = 0.120°) and 51.7° (FWHM = 0.192°), respectively; with a D-spacing distance of 2.03 Å for the plane (1 1 1) and 1.76 Å for the (2 0 0) plane. The (1 1 1) / (2 0 0) planes ratio for pure Ni is 5.61 while in Ni/Ag and Ni/Cu catalysts is 10.5 showing a predominance of (1 1 1) planes. After the spontaneous deposition of metals, the amount of (2 0 0) planes decrease. It is reported in literature that the nickel (1 1 1) planes are more stable than the (2 0 0) ones, which explains why the reduction of metals such as Cu and Ag occurs on top of the (2 0 0) nickel planes [18].

On the other hand, the peaks corresponding to Cu or Cu oxides are not observed in the Ni/Cu_f diffractogram because these peaks are masked by the Ni (1 1 1) peaks [32,33], while in the Ni/Ag_f diffractogram a signal corresponding to metallic Ag at 38.1° is observed (Fig. 4b).

3.3. Cyclic voltammetric and chronoamperometric analysis

3.3.1. Freshly synthesized catalysts

Fig. 5(a) shows a typical cyclic voltammogram obtained for Ni/Ag_f and Ni/Cu_f, measured at 298 K in 1 M KOH solution with a scan rate of 10 mV s^{-1}. It can be seen that the onset potential (OP) for HER on Ni/Ag_f is ~−1.1 V (vs. SCE), similar to that found on pure Ni electrodes [8,23,34], while the OP observed on Ni/Cu_f is ~−0.9 V (vs. SCE).

The fact that the Ni/Cu current density (at −1.5 V vs SCE) is lower than the observed in Ni/Ag even considering that the Ni/Cu OP is around 0.2 V lower, is due to two opposing effects: The D-band position of Cu, being closer to the Fermi level than the observed on Ag and the weaker coupling of Cu respect to Ag (which in a pure state has a more expanded D-band) could be the reason why the Ag is favored as catalyst [18].

In Fig. 5(b) a magnification of the cyclic voltammetry of Ni/Ag_f and Ni/Cu_f electrodes is presented. For Ni/Ag_f, one cathodic peak (I_c) and two anodic peaks (I_{a1} and I_{a2}) are observed (marked with arrows).

The I_{a1} peak is normally associated with the Ni reaction to form α-$Ni(OH)_2$ (according to Eq. (5)), with subsequent dissolution of the hydrogen incorporated into the Ni. The I_c peak involves the reduction of α-$Ni(OH)_2$ to form Ni and water discharge during the HER, and it appears at lower potential in Ni/Cu_f due to lower OP of that catalyst. This peak as well as the I_{a1} peak appears at lower overpotentials in Ni/Cu electrodes [35,36].

$$Ni_{(s)O} + xH_2O_{(l)} + xe^- \rightleftarrows \alpha - NiH_{x(s)} + xOH^-_{(aq)} \quad (5)$$

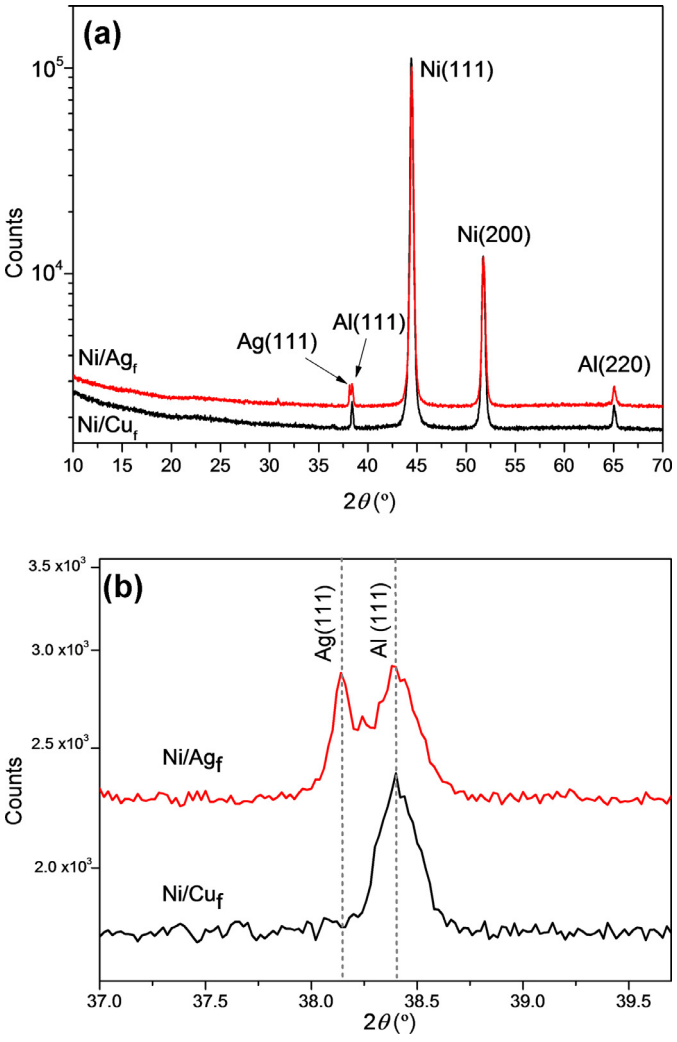

Fig. 4. (a) X-ray diffraction patterns of Ni/Ag$_f$ and Ni/Cu$_f$. (b) Magnification of the X-ray diffraction patterns presented in (a).

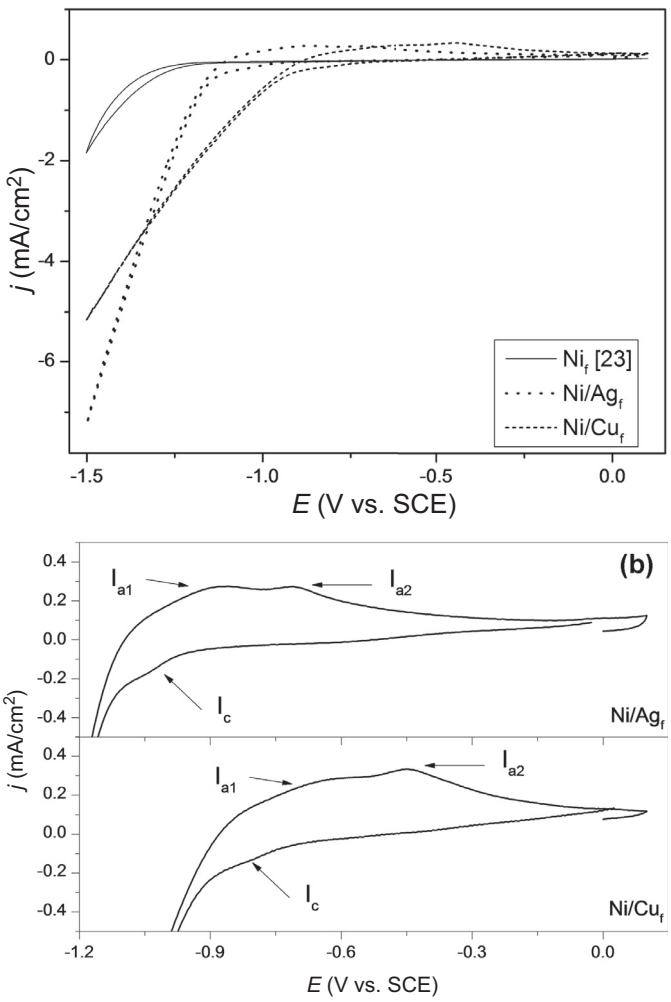

Fig. 5. (a) Cyclic voltammograms of Ni/Ag$_f$ and Ni/Cu$_f$ catalysts in 1 M KOH at 298 K (scan rate: 10 mV s^{-1}). (b) Magnification of the cyclic voltammograms presented in (a).

The I_{a2} peak is an oxidation peak that usually is absent with pure Ni electrodes. Additionally, in the voltammogram of Ni/Cu electrode the I_{a2} peak appears at an overpotential 0.27 V lower than that of the Ni/Ag electrode, while the difference in the onset potentials of both catalysts is 0.20 V. This indicates that the shift of this peak value is not only due to the change in the OP, but also involves oxidation of different species. Then, we conclude that the I_{a2} peaks are due to oxidation of Ag and Cu in Ni/Ag and Ni/Cu respectively, and the difference in the I_{a2} peak potential is due to the higher oxidation overpotential of Cu compared to Ag [27].

3.3.2. Short aged catalysts

The Ni/Ag$_f$ and Ni/Cu$_f$ electrodes, after being characterized with different electrochemical techniques (LSV by RDE and cyclic voltammetry at different temperatures, and EIS at different potentials), were subjected to a short-term ageing process employing a 4 h chronoamperometric pulse at −1.5 V (vs. SCE) in 1 M KOH solution. This procedure was employed in order to analyze the effect of the hydrogen evolution over the electro-catalytic activity of the electrodes. No appreciable changes in color and structure were observed on the electrodes surfaces or the electrolyte after the short ageing procedure. Fig. 6(a) shows the hydrogen evolution chronoamperometry transients, recorded on both catalysts, which exhibit current densities higher than the observed in commercial pure Ni electrodes [23]. Furthermore, it can be seen that the Ni/Cu has a higher current density than the Ni/Ag, and a gradual decrease of the hydrogen generation current is observed.

The electrode deactivation rate was calculated as [37,38]:

$$\delta = -\frac{100}{j_e}\left(\frac{\mathrm{d}j}{\mathrm{d}t}\right) \tag{6}$$

where j_e is the current extrapolated at the start of polarization, and the slope, dj/dt, is evaluated from the linear decay at $t >$ 2000 s. The decay rate obtained for the Ni/Ag and Ni/Cu were 7.5 × 10^{-4} s^{-1} and 4.0 × 10^{-4} s^{-1}, respectively. This implies that the Ni/Ag has not only lower electrocatalytic activity than the Ni/Cu, but also deactivates faster due to the ageing process. As comparison, the decay rate measured for bare nickel is 1.5 × 10^{-3} s^{-1}, indicating a decrease of the decay rate to a half of the bare Ni value when Ag is used as plating metal, and almost a quarter when Cu is used as surface modifier.

The aged Ni/Ag and Ni/Cu catalysts (denoted as Ni/Ag$_a$ and Ni/Cu$_a$, respectively) were characterized by the same electrochemical techniques used for the characterization of freshly synthesized samples.

In Fig. 6(b) the comparison of cyclic voltammograms for Ni/Ag and Ni/Cu (before and after ageing) is shown. It can be seen that the Ni/Ag catalyst maintains its OP after ageing, although the current density (at −1.5 V vs. SCE) diminishes by 40%, showing a clear deactivation of the electrode. On the other hand, the Ni/Cu

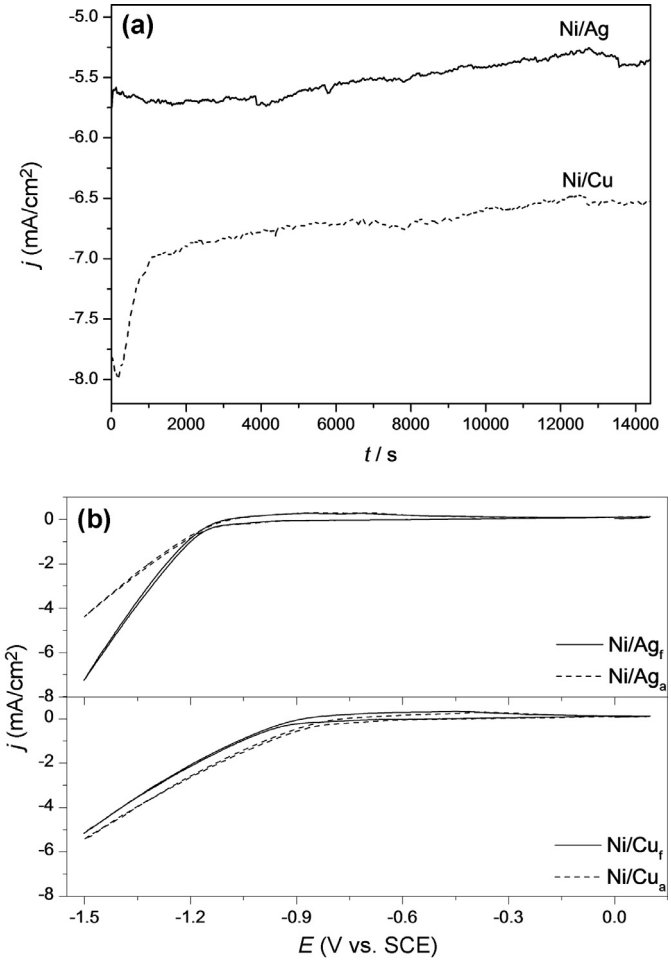

Fig. 6. (a) Chronoamperometric profile of hydrogen evolution reaction on Ni/Ag_f and Ni/Cu_f in 1 M KOH obtained at −1.5 V (vs. SCE). 298 K. and rotation speed of 900 rpm. (b) Comparison of cyclic voltammograms of fresh and aged catalysts in 1 M KOH at 298 K (scan rate: 10 mV s^{-1}).

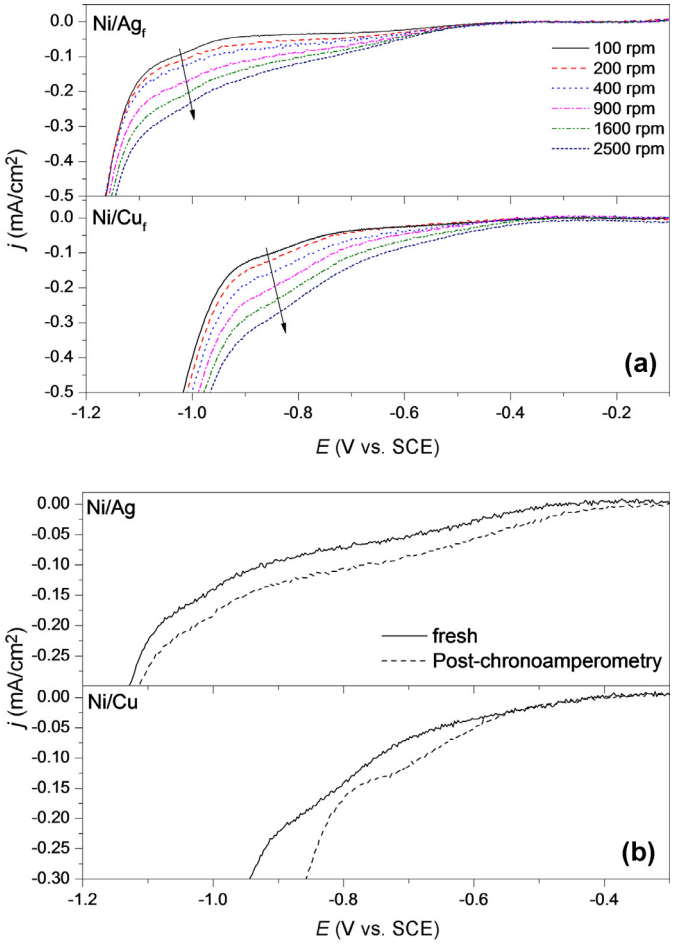

Fig. 7. (a) Current potential curves for HER obtained in 1 M KOH at 298 K on Ni/Ag_f and Ni/Cu_f at different rotation rates. (b) LSV of fresh and ageing catalysts in 1 M KOH measured at 298 K (Rotation rate: 900 rpm, Scan rate: 10 mV s^{-1}).

catalyst decreases their OP ca. 0.1 V after ageing and, although is not clearly observed in Fig. 6(b), there is a deactivation electrode evidenced by the decreasing slope (dj/dV) of the hydrogen evolution curve by 15%, which is compensated by the decrease in the OP of the reaction. Thus, although both catalysts suffer a deactivation in their capability to catalyze the HER, Ni/Cu catalyst exhibits a decrease in OP which makes it more electrochemically active than Ni/Ag. This decrease in the OP of Ni/Cu may be due to the fact that CuO_x is reduced to metallic Cu during the generating hydrogen process, and the oxide has a binding energy with H greater than that of Ag [27], enhancing the tendency of water to discharge on its surface to facilitate the Volmer reaction.

It is important to point out that, unlike what was observed in the CV measurements on fresh catalysts, where the NiAg had a higher current density at −1.5 V than the NiCu, during chronoamperometric measurements the NiCu catalyst showed a higher current density at −1.5 V than the NiAg, similar to that observed in the CV measurements carried out on the aged catalysts. This indicates that the changes caused by ageing during chronoamperometry are evidenced by CV and EIS in the latest experiments.

3.4. RDE

In Fig. 7(a) a set of RDE current density-potential curves, obtained on Ni/Ag_f and Ni/Cu_f catalysts in 1 M KOH at 298 K in the cathodic scan, is presented. It is important to remark that the RDE measurements by LSV showed similar profiles in both cathode and anode scans. Both catalysts show a well-defined charge transfer kinetic control at potentials above −0.50 and −0.40 (vs. SCE) for Ni/Ag_f and Ni/Cu_f, respectively. Significant differences between the electrochemical behavior of Ni/Ag_f and Ni/Cu_f catalysts are observed. A mixed kinetic-diffusion control occurs in the range of −0.7 to −0.50 V (vs. SCE) for Ni/Ag_f catalyst. The mixed kinetic-diffusion control in Ni/Cu_f is less defined than in the case of Ni/Ag_f, due to the narrow diffusional control range presented by the electrode (−0.7 to −0.9 V vs. SCE). Additionally, the diffusional control area increases after the ageing process due to the stabilization of the electrode (not shown), as was presented in a previous work [24].

A dependence of the current density with the rotation rate is observed. Fig. 7(b) shows RDE current density-potential curves for each catalyst before and after the short-term ageing measured at 900 rpm. In the case of the Ni/Ag catalyst an increase in the cathodic current is observed, while the OP remains practically constant. Meanwhile, the Ni/Cu catalyst shows a substantial change in the electrochemical response after ageing. It can be seen a decrease of approximately 0.20 V in the OP, and a rather marked diffusional control range (between 0.7 and 0.8 V), as compared to that observed in the fresh catalyst.

In Fig. 8 the Koutecky–Levich graphics measured at 298 K for each catalyst at different potentials are shown and compared to the theoretical curve for the one electron transference (dashed line). The linearity of the plot indicates that HER is a first order

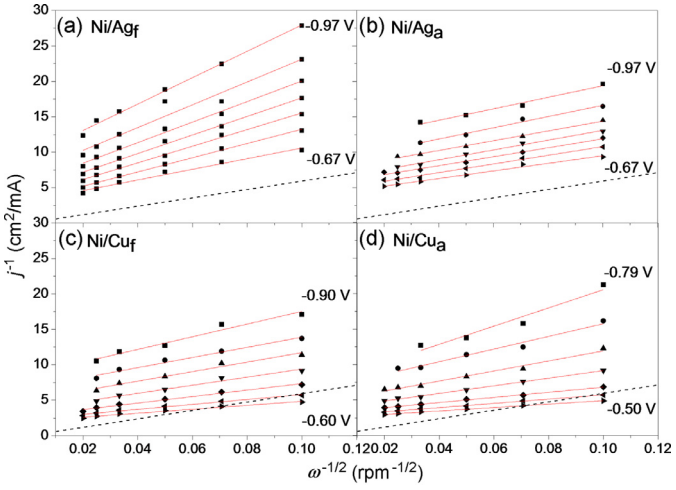

Fig. 8. K-L plots for HER at 298 K on (a) Ni/Ag$_f$ (b) Ni/Ag$_a$ (c) Ni/Cu$_f$ and (d) Ni/Cu$_a$ at different electrode potentials. The theoretical one electron slope is showed as a dashed line.

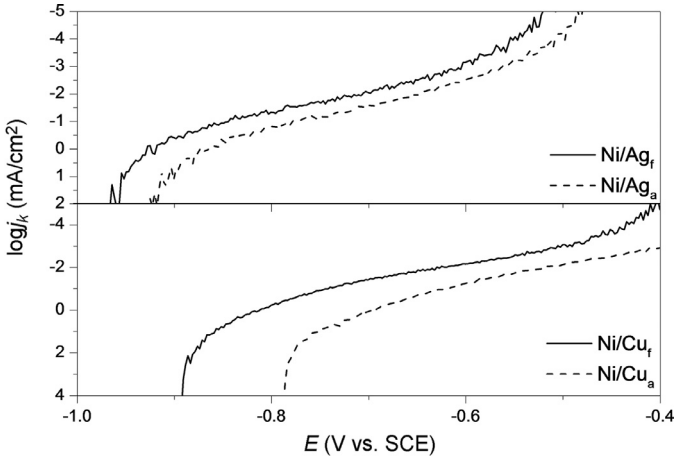

Fig. 9. Mass transfer corrected Tafel plots for the HER on fresh and aged catalysts measured at 1600 rpm and 293 K. Scan rate = 10 mV s^{-1}.

reaction and a change in j_k (obtained from the $\omega^{-1/2} = 0$ interception) is observed in all the cases [39]. It can be seen that all catalysts show an increase in the electron transfer rate with increasing overpotential [39], which is consistent with the Volmer reaction being the rate determining step of the global reaction. The Levich slope (B) and transferred electrons number (n) obtained from the analysis at 298 K are summarized in Table 1. It is important to note that n values do not correspond only to the HER, but cover all reactions occurring in the potential range, such as, copper or silver oxidation/reduction and nickel hydride formation, and constitutes only an indicative of what is happening on the surface. It is observed that for Ni/Ag and Ni/Cu electrodes the number of electrons transferred (n) increases with ageing the catalysts, which is a behavior usually observed in Ni-based catalysts [23,24]. The high value of n would be indicative of a contribution of the Heyrovsky reaction in the overall mechanisms, or the presence of a second reaction (as the formation of Cu oxides). There are several studies that show that the Heyrovsky reaction does not occur in the presence of Cu [40–42] and the Volmer reaction only contributes to the reaction rate in the overall process. This evidence, coupled with the preferential presence of oxygen in Cu cubic particles observed in the EDX mapping indicates that $n > 1$ is due to the parallel reaction, even in the aged catalysts.

Fig. 9 shows the diffusion corrected Tafel curves measured for each catalyst at 900 rpm and 298 K. Different Tafel slopes values were obtained for each catalyst, fresh and aged, which are summarized in Table 1. The obtained Tafel slope values are similar to that reported in literature for pure Ni (0.13 V dec^{-1}) [23,43].

It can be seen in Table 1 that the fresh catalysts exhibit a higher Tafel slope value than that of pure Ni, while the slope obtained for the aged catalysts is 0.126 V dec^{-1} in both cases. This indicates that, besides the hydrogen generation process, the HER mechanism for the fresh catalysts involves other processes, such as the oxidation of copper or silver. The changes observed in the value of the Tafel slope are consistent with the differences observed in the CV of Fig. 6(b).

Furthermore, in Fig. 9, the Ni/Cu catalyst shows a change in Tafel slope at low overpotential values that is not observed in the Ni/Ag catalyst, evidence that can be related to the existence of a second reaction different to HER. Probably, the change in the Tafel slope is more evident for the Ni/Cu catalyst when compared with the Ni/Ag catalyst, due to the higher tendency of Cu to form oxides.

The exchange current values (j_0) obtained at 298 K and 900 rpm are presented in Table 1. It can be seen that in all cases these values are higher than those presented for bare Ni electrodes. Both catalysts show small changes in the j_0 after ageing, contrary to the strong deactivation observed in pure Ni, where j_0 decreases by two orders of magnitude [23]. This is an indication that deactivation by hydride formation is clearly diminished by the use of Cu and Ag on Ni catalysts.

3.5. EIS

Both electrodes exhibited similar depressed “semicircular” capacitive arcs (i.e., circular arcs with their center below the real axis) at all potentials in the explored frequency. This frequency response is typical of a single-step charge transfer reaction kinetically controlled without diffusion control in the time domain corresponding to the frequency range of the measurements [44,45].

The general equation for the HER predicts the formation of two ideal semicircles on the impedance plane plots with an overpotential dependent radius [45,46]. However, usually only one ideal semicircle appeared, because the charge transfer dominated the frequency response.

Different authors propose the exchange of a capacity element for a constant phase element (CPE) due to the inhomogeneity and/or the roughness of the electrode surface [44,47]. CPE is one of the most frequently employed distributed element and may be associated with a distribution of relaxation times or activation

Table 1. Kinetic parameters for the HER on the synthesized catalysts in 1 M KOH, Tafel slope, Levich slope (B) and number of electrons (n) calculated at 298 K, and exchange current density. Moreover, pure nickel data are also presented.

	Ni/Ag$_f$	Ni/Ag$_a$	Ni/Cu$_f$	Ni/Cu$_a$	Ni$_f$ [23]	Ni$_a$ [23]
b/V dec^{-1}	−0.145	−0.126	−0.139	−0.126	−0.256	−0.142
B/mA cm^{-2} rpm$^{-1/2}$	73.1	59.2	50.6	38.4	–	–
n	0.81	1.00	1.17	1.54	1	0.64
j_0/mA cm^{-2}	4.46 × 10^{-4}	5.34 × 10^{-4}	2.45 × 10^{-4}	9.42 × 10^{-5}	1.2 × 10^{-4}	6.91 × 10^{-7}
dj/dV/mA cm^{-2} V^{-1}	23.0	13.0	10.6	9.8	–	–

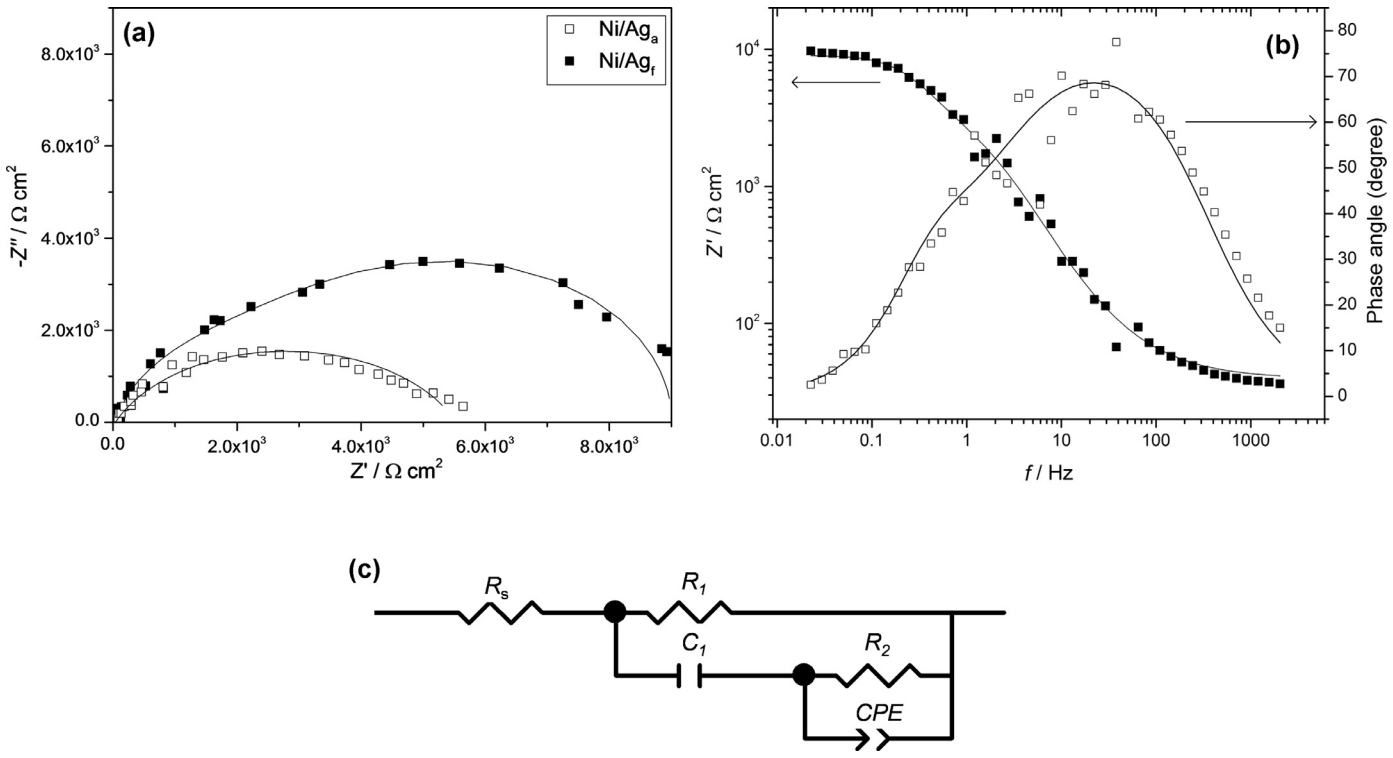

Fig. 10. (a) Nyquist plot Impedance spectra in the complex plane for the HER on Ni/Ag$_f$ (filled dots) and Ni/Ag$_a$ (open dots). (b) Bode plot for the Ni/Ag$_f$ catalyst in 1 M KOH at 298 K and at a rotation rate of 900 rpm at the OCP. The filled square corresponds to *Z*' and the open squares corresponds to the measured phase angle. The solid lines are calculated using the modified AHEC. (c) Modified Armstrong and Henderson equivalent circuit.

energies on the electrode surface [48–51]. The analysis of impedance with equivalent schemes including CPE, often considered very formal, was employed here to obtain a proper fit of the resistances (R_1 and R_2) to be used below for Tafel analysis while in analysis we avoided the analysis of the capacitances.

Fig. 10(a) shows the corresponding EIS in the complex plane recorded at the open circuit potential ($E = -0.35$ V), for Ni/Ag$_f$ and Ni/Ag$_a$ measured at 298 K and 900 rpm. Similar plots for Ni/Cu$_f$ and Ni/Cu$_a$ are presented in the Supporting information (Fig. S3). Fig. 10(b) shows the corresponding Bode diagram to the spectrum at the onset potential for Ni/Ag$_f$ and the fit obtained using a modified Armstrong and Henderson equivalent circuit (AHEC) [46], by changing the pseudo capacitance by a CPE component to obtain a satisfactory fit [52].

Both catalysts show a similar behavior, which is consistent with a charge transfer controlled process [34]. Fig. 10(c) shows the modified AHEC, where R_s is the solution resistance, R_1 is the charge transfer resistance for the electrode reaction, C_1 the double layer capacitance, R_2 is related to the superficial mass transfer resistance of H_{ad}.

The impedance spectra in the complex plane were also determined at three electrode potentials values, selected to cover the entire HER region: the onset potential of the HER (for each catalyst), and overpotentials of 0.1 V and 0.3 V more cathodic than the OP. There is a noticeable change in the charge transfer resistance and capacitance after the ageing process. Variations in the capacitance may be associated with a change in the type of H adsorption, related with the hidruration of the surface.

Data in Table 2 show that after ageing of Ni/Ag and Ni/Cu catalysts, there is an increase of the charge transfer resistances that occurs at the potential of HER (onset potentials and higher overpotentials). This increase in charge transfer resistance is consistent with the decrease in the d*j*/d*V* slope and the resulting decrease in current density after ageing, shown in Table 1. Additionally, the

Table 2. Parameters of the modified AHEC for the HER in 1 M KOH at 298 K.

Catalyst	*E*/V (SCE)	R_1/ Ω cm^2	R_2/Ω cm^2	C_p/F cm^{-2}	CPE/F cm^{-2}
Ni/Ag$_f$	−0.36 (OCP)	9079	4106	4.92×10^{-5}	6.85×10^{-5}
	−0.97 (OP)	5377	1667	0.00117	1.63×10^{-4}
Ni/Ag$_a$	−0.35 (OCP)	7141	1148	4.95×10^{-5}	8.59×10^{-5}
	−0.97 (OP)	741.9	938.7	0.00193	2.37×10^{-4}
Ni/Cu$_f$	−0.35 (OCP)	15,084	4415	2.66×10^{-5}	4.42×10^{-4}
	−0.9 (OP)	400.3	167.3	4.06×10^{-5}	9.61×10^{-4}
Ni/Cu$_a$	−0.35 (OCP)	17,733	4378	6.63×10^{-5}	9.42×10^{-5}
	−0.79 (OP)	707.2	318.6	8.21×10^{-5}	3.92×10^{-4}

Ni/Cu catalyst has greater resistance than the Ni/Ag catalyst, which is according to the greater tendency to oxidation of Cu compared to Ag.

The sum $R_1 + R_2$ (at each potential) represents the total faradaic resistance which is related with the kinetics of HER, and its reciprocal is directly related to the faradaic current density. Since the HER is charge transfer controlled within the considered potential region, the *E* vs. log $(R_1 + R_2)^{-1}$ plot is linear, and its slope equal to the Tafel slope, *b*. Fig. 11(a) and (b) shows the Tafel plot (without mass transfer correction) along with the simulated *E* vs. $\log(R_1+R_2)^{-1}$ plot for Ni/Ag$_f$ and Ni/Ag$_a$ catalysts. The graphs obtained for fresh and aged Ni/Cu catalysts (not showed) are similar to those presented in Fig. 11. The separation between the Tafel curve (log *j*) and the $\log(R_1 + R_2)^{-1}$ observed for all the catalysts (fresh and aged) was 1.30 ± 0.1, close to the theoretical separation for Langmuir type adsorption (1.289) [53]. Changes in the adsorption type are not observed after ageing, unlike what is found in pure Ni catalysts where, after ageing, a Temkin type adsorption, characterized by a theoretical separation of 1.86, is observed [53].

Temkin type hydrogen adsorption is associated with the formation of a nickel hydrides layer, responsible for the loss of electrocatalytic activity [23,54]. The maintaining of the Langmuir

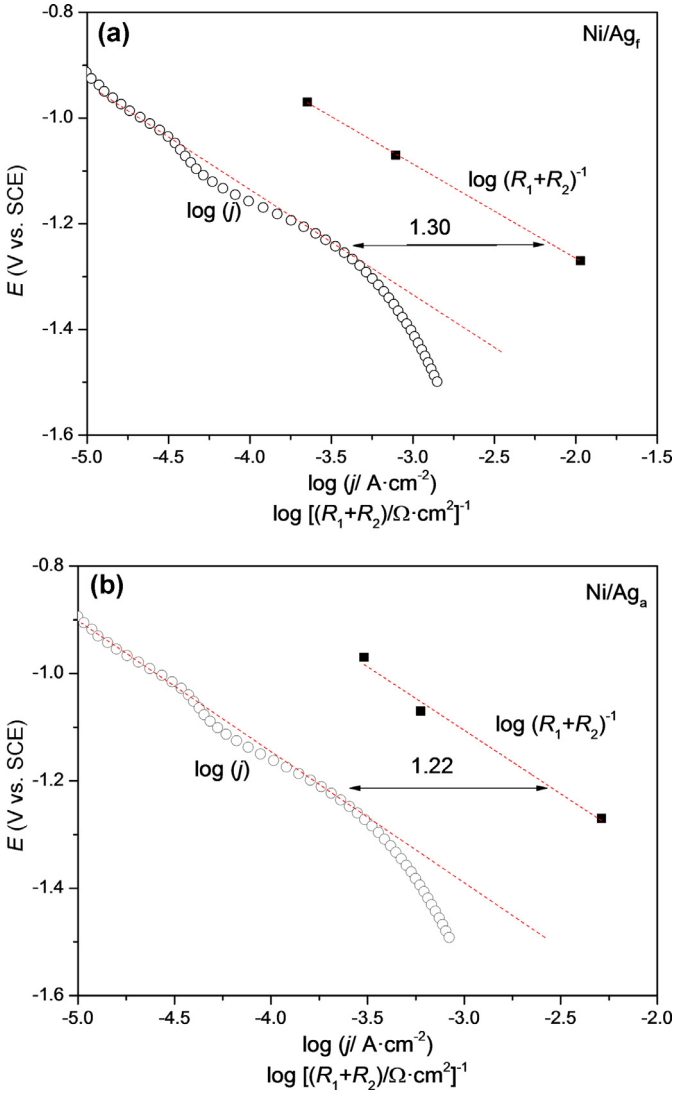

Fig. 11. Experimental Tafel plot (circled points) and simulated E-log$(R_1+R_2)^{-1}$ plot (squares) with the corresponding linear fit (dashed line) for the HER in 1 M KOH solution at 298 K, on (a) Ni/Ag$_f$ and (b) Ni/Ag$_a$.

adsorption type on the catalyst surface after the ageing process is consistent with a decrease in hydride formation.

4. Conclusions

In this paper the mechanism of hydrogen evolution reaction on Ni/Ag and Ni/Cu electrodes synthesized via spontaneous deposition is analyzed. The results of EIS and RDE electrochemical characterization of the HER on a freshly synthesized and a short-term aged catalyst are discussed.

The complementation of the RDE analysis with impedance spectroscopy allows us to analyze the changes in the hydrogen adsorption. A Langmuir adsorption type was found for all the Ni/Ag and Ni/Cu catalysts, fresh and aged. This behavior is considerably different from those found in pure nickel were, after ageing, a Temkin type adsorption appears, related to the formation of superficial nickel hydrides. The different adsorption behavior can be responsible for the invariance of the HER onset potential for the modified nickel catalysts, unlike that found in pure Ni were the onset potential in aged Ni is 0.2 V higher than the corresponding value for fresh polished/degreased Ni. Hence we conclude that the modification of Ni with Cu and Ag prevents the electrode deactivation.

The use of transition metals with a $xd^{10}(x+1)s^1$ structure such as Cu ($3d^{10}4s^1$) and Ag ($4d^{10}5s^1$) deposited on Ni modifies catalytic activity for the hydrogen electrochemical generation, but only in the case of Ni/Cu a decrease of the onset potential of HER is observed. Is observed that the hydrogen evolution rate is almost the same on Cu and Ag.

The synthesized catalysts exhibited greater stability and improved electrochemical activity in conditions of hydrogen generation, where the pure Ni usually shows clear signs of activity loss.

Acknowledgments

The authors thank financial support from Agencia Nacional de Promoción Científica y Tecnológica (PICT 1818), and CONICET (PIP 00095). H.R.C., G.I.L., and E.A.F. are permanent research fellows of CONICET. The authors thank to LAMARX laboratory for its assistance in SEM/EDX measurements, and to Dr. Raúl Carbonio and Dra. Cecilia Blanco for XRD measurements.

Supplementary materials

Supplementary material associated with this article can be found, in the online version, at doi:10.1016/j.jechem.2016.10.009.

References

[1] G. Gahleitner, Int. J. Hydrogen Energy 38 (2013) 2039–2061.
[2] D. Pletcher, L. Xiaohong, Int. J. Hydrogen Energy 36 (2011) 15089–15104.
[3] J.O.M. Bockris, Int. J. Hydrogen Energy 38 (2013) 2579–2588.
[4] W. Lubitz, W. Tumas, Chem. Rev. 107 (2007) 3900–3903.
[5] L.M. Doubova, S. Trasatti, J. Electroanal. Chem. 467 (1999) 164–176.
[6] H. Hu, M. Qiao, Y. Pei, K. Fan, H. Li, B. Zong, X. Zhang, Appl. Catal. Gen. 252 (2003) 173–183.
[7] R. Solmaz, A. Döner, G. Kardas, Electrochem. Commun. 10 (2008) 1909–1911.
[8] I. Bianchi, E. Guerrini, S. Trasatti, Chem. Phys. 319 (2005) 192–199.
[9] D.S.P. Cardoso, S. Eugénio, T.M. Silva, D.M.F. Santos, C.A.C. Sequeira, M.F. Montemor, RSC Adv. 5 (2015) 43456–43461.
[10] Y. Zhu, X. Zhang, J. Song, W. Wang, F. Yue, Q. Ma, Appl. Catal. Gen. 500 (2015) 51–57.
[11] J. Wang, W. Cui, Q. Liu, Z. Xing, A.M. Asiri, X. Sun, Adv. Mater. 28 (2016) 215–230.
[12] D. Zhou, L. He, W. Zhu, X. Hou, K. Wang, G. Du, C. Zheng, X. Sun, A.M. Asirid, J. Mater. Chem. A, doi:10.1039/c6ta03628g.
[13] L.L. Feng, G. Yu, Y. Wu, G.D. Li, H. Li, Y. Sun, T. Asefa, W. Chen, X. Zou, J. Am. Chem. Soc. 137 (2015) 14023–14026.
[14] X. Zou, Y. Zhang, Chem. Soc. Rev. 44 (2015) 5148–5180.
[15] J. Tian, Q. Liu, A.M. Asiri, X. Sun, J. Am. Chem. Soc. 136 (2014) 7587–7590.
[16] J. Garche, Encyclopedia of Electrochemical Power Sources, 1, Elsevier, Amsterdam, 2009, p. 751.
[17] E. Santos, W. Schmickler, Angew. Chem. Int. Ed. 46 (2007) 8262–8265.
[18] P. Quaino, F. Juarez, E. Santos, W. Schmickler, Beilstein J. Nanotechnol. 5 (2014) 846–854.
[19] B.E. Conway, E.M. Beatty, P.A.D. Demaine, Electrochim. Acta 7 (1962) 39–54.
[20] S. Sharifi-Asl, D.D. Macdonald, J. Electrochem. Soc. 160 (2013) H382–H391.
[21] Z. Yin, F. Chen, J. Power Sources 265 (2014) 273–281.
[22] M.H. Tang, C. Hahn, A.J. Klobuchar, J.W. Desmond Ng, J. Wellendorff, T. Bligaard, T.F. Jaramillo, Phys. Chem. Chem. Phys. 16 (2014) 19250–19257.
[23] E.A. Franceschini, G.I. Lacconi, H.R. Corti, Electrochim. Acta 159 (2015) 210–218.
[24] E.A. Franceschini, G.I. Lacconi, H.R. Corti, Int. J. Hydrogen Energy 41 (2016) 3326–3338.
[25] J. Rodríguez-Carvajal, J. Phys. B 192 (1993) 55–56.
[26] E.A. Franceschini, M.M. Bruno, F.A. Viva, F.J. Williams, M. Jobbágy, H.R. Corti, Electrochim. Acta 71 (2012) 173–180.
[27] W.M. Haynes, CRC Handbook of Chemistry and Physics, 94th ed., CRC Press, Boca Raton, FL, 2003.
[28] S. Trasatti, O.A. Petrii, Pure Appl. Chem. 63 (1991) 711–734.
[29] L. Vázquez-Gómez, S. Cattarin, P. Guerriero, M. Musiani, Electrochim. Acta 53 (2008) 8310–8318.
[30] S.L. Xu, X.Y. Song, C.H. Fan, G.Z. Chen, W. Zhao, T. You, S.X. Sun, J. Cryst. Growth 305 (2007) 3–7.
[31] M.D. Susman, Y. Feldman, A. Vaskevich, I. Rubinstein, ACS Nano 8 (2014) 162–174.
[32] K. Ngamlerdpokin, N. Tantavichet, Int. J. Hydrogen Energy 39 (2014) 2505–2515.
[33] T.M.D. Dang, T.T.T. Le, E. Fribourg-Blanc, M.C. Dang, Adv. Nat. Sci. Nanosci. Nanotechnol. 2 (2011) 025004–025010.

[34] A. ðukic, V. Alar, M. Firak, S. Jakovljevic, J. Alloy Compd. 573 (2013) 128–132.
[35] D.S. Hall, C. Bock, B.R. MacDougall, J. Electrochem. Soc. 160 (2013) F235–F243.
[36] Z. Szklarska-Smialowski, M. Smialowski, J. Electrochem. Soc. 110 (1963) 444–448.
[37] E.A. Franceschini, M.M. Bruno, F.J. Williams, F.A. Viva, H.R. Corti, ACS Appl. Mater. Interfaces 5 (2013) 10437–10444.
[38] M.M. Bruno, E.A. Franceschini, G.A. Planes, H.R. Corti, J. Appl. Electrochem. 40 (2010) 257–263.
[39] R.W. Zurilla, R.K. Sen, E. Yeager, J. Electrochem. Soc. 125 (1978) 1103–1109.
[40] A.T. Kuhn, C.J. Mortimer, G.C. Bond, J. Lindley, J. Electroanal. Chem. 34 (1972) 1–14.
[41] A. Ruderman, M.F. Juarez, G. Soldano, L.B. Avalle, G. Beltramo, M. Giesen, E. Santos, Electrochim. Acta 109 (2013) 403–410.
[42] A. Ruderman, M.F. Juarez, L.B. Avalle, G. Beltramo, M. Giesen, E. Santos, Electrochem. Commun. 34 (2013) 235–238.
[43] G. Kreysa, B. Hakansson, P. Ekdunge, Electrochim. Acta 33 (1988) 1351–1357.
[44] E. Daftsis, N. Pagalos, A. Jannakoudakis, P. Jannakoudakis, E. Theodoridou, R. Rashkov, M. Loukaytsheva, N. Atanassov, J. Electrochem. Soc. 150 (2003) C787–C793.
[45] D.A. Harrington, B.E. Conway, Electrochim. Acta 32 (1987) 1703–1712.
[46] R.D. Armstrong, M. Henderson, J. Electroanal. Chem. 39 (1972) 81–90.
[47] G.J. Brug, A.L.G. Van Den Eeden, M. Sluyters-Rehbach, J.H. Sluyters, J. Electroanal. Chem. Interfacial Electrochem. 176 (1984) 275–295.
[48] A. Lasia, Modern Aspects of Electrochemistry, 32, Kluwer Academic/Plenum Publishers, New York, 1999, p. 143.
[49] U. Rammelt, G. Reinhard, Electrochim. Acta 35 (1990) 1045–1049.
[50] T.J. Pajkossy, Electroanal. Chem. Interfacial Electrochem. 300 (1991) 1–11.
[51] P. Heiduschka, A.W. Munz, W. Gopel, Electrochim. Acta 39 (1994) 2207–2223.
[52] A. Damian, S. Omanovic, J. Power Sources 158 (2006) 464–476.
[53] L. Bai, D.A. Harrington, B.E. Conway, Electrochim. Acta 32 (1987) 1713–1731.
[54] D.S. Hall, D.J. Lockwood, S. Poirier, C. Bock, B.R. MacDougall, ACS Appl. Mater Interfaces 6 (2014) 3141–3149.